RSC Advances

PAPER

View Article Online
View Journal | View Issue

Cite this: *RSC Adv.*, 2017, **7**, 7996

Application of magnetic Cd^{2+} ion-imprinted mesoporous organosilica nanocomposites for mineral wastewater treatment

Shuibin Cen,[a] Weiming Li,[c] Shiying Xu,[d] Zhihong Wang,[d] Youwen Tang,*[d] Haishui Wang*[a] and Chaohai Wei[b]

Received 2nd December 2016
Accepted 16th January 2017

DOI: 10.1039/c6ra27679b

www.rsc.org/advances

This work demonstrates a simple strategy for producing highly selective adsorption magnetic ion imprinted mesoporous silica (MIIMS) nanocomposites. They have been functionalized by a γ-(aminoethylamino) propyl chelating group for specific recognition and rapid removal of toxic heavy metal ions from wastewaters. The superparamagnetic Fe_3O_4 nanocrystal was encapsulated in an imprinted mesoporous organosilica shell *via* a co-condensation synthesis method. The results of transmission electron microscopy (TEM) and small angle X-ray diffraction (XRD) confirmed that the imprinted mesoporous organosilica shell preserved a highly ordered 2D mesostructure. The Brunauer–Emmett–Teller (BET) analysis found the surface area was 946 $m^2\ g^{-1}$. The saturated adsorption capacity of MIIMS toward cadmium reached up to 25.2 mg g^{-1} (0.224 mmol g^{-1}) at pH 5.0. The adsorption of cadmium reached an equilibrium within 4.5 min. The results of a selectivity study revealed that the adsorption capacity for Cd^{2+} is much high than other co-existing heavy metal ions. The adsorption efficiency of MIIMS was above 94.2% after six extraction-stripping cycles. The MIIMS can efficiently remove cadmium ions in water treatment applications.

1. Introduction

Cadmium is a toxic metal element that causes serious health hazards to humans and has been considered as one of the most serious environmental pollutants. Prolonged exposure to cadmium can very likely cause renal dysfunction, diabetes, cardiovascular diseases and cancers even at a very low concentration.[1,2] Many researches have confirmed that cadmium can be transferred from water to plants and to human bodies. Some industrial effluents, such as mining wastewater and waste electroplating solutions, which often have complicated chemical compositions, are the major sources of environmental cadmium pollution.[3] Therefore, developing an economic and effective method to remove cadmium from contaminated water is a vital requirement.

Plenty of methods for the uptake and elimination of Cd^{2+} have been put forward, including chemical precipitation, ion exchange, electrochemical treatment, membrane filtration, and adsorption.[4–10] Among them, adsorption has attracted growing attentions due to its high efficiency, operation convenience, and environmental friendliness.[11] A variety of adsorption materials, *viz.* activated carbon, polymeric resins, organoclays, humic acids and plants have been developed to remove Cd^{2+} from contaminated aqueous systems.[12] However, several limitations, such as very long adsorption and separation time, low uptake affinity or high cost of manufacturing have inhibited their applications in real environment. Thus, developing of new adsorption materials with high efficiency, wide range of applicability and low cost has become important.

Mesoporous silica has been explored widely as adsorbents of organic compounds, biomolecules and heavy metals due to their large surface area, tunable porosity, uniform pore-size-distribution, controlled morphology and high stability.[13–17] However, the anti-interference ability of mesoporous silica in complex samples is relatively poor, which severely hinders its practical applications in water treatment.

Molecularly imprinted polymers (MIPs) have been used as solid phase extraction adsorbents because they possess binding sites with selective recognition capability toward a given target molecule.[18] In general, MIPs offer high selectivity, low cost, durability and reusability. Therefore, molecular imprinting has become a well-recognized powerful technique in recent years for developing efficient adsorbents for wastewater treatment.[19,20] However, traditional metal ion imprinted polymers (MIIPs) exhibit a low adsorption capacity and poor site accessibility to

[a]*School of Chemistry and Chemical Engineering, South China University of Technology, Guangzhou 510641, China. E-mail: wanghsh@scut.edu.cn*

[b]*The Key Lab of Pollution Control and Ecosystem Restoration in Industry Clusters, Ministry of Education, South China University of Technology, Guangzhou, China*

[c]*Technical Service Center Laboratory of Panyu Entry–Exit Inspection & Quarantine Bureau, Guangzhou, China*

[d]*MOE Key Laboratory of Laser Life Science, School of Chemistry and Environment, South China Normal University, 510631, Guangzhou, China. E-mail: tanglab@scnu.edu.cn*

the target because the binding sites are typically embedded within a highly cross-linked polymer matrix.

Metal ion imprinted mesoporous silica had also been reported in the past.[21] Commonly, the mesoporous silica materials can be modified by co-condensation[22] and grafting.[23] Co-condensation modification involves simultaneous addition of corresponding silica and structure-directing agents (SDAs) with organosilica precursors and template, where the organo-functional groups covalently anchor in the pore walls,[24] which can effectively overcome some shortcomings of the grafting synthesis, such as loss of surface area, pore blocking, and heterogeneous distribution of recognition sites.[25] Recently, highly ordered metal ion imprinted mesoporous silica have been synthesized by co-condensation for heavy metal wastewater treatment.[26] Those nanoparticles with small particle sizes are more advantageous with respect to adsorption equilibrium and kinetics. However, separation of certain substances from multiphase complex systems by ion imprinted mesoporous silica is quite troublesome, introducing certain restrictions in the use of these adsorbents.

In recent years, magnetic mesoporous silica has been extensively investigated due to their combination of multifunctional mesoporous structure and inherent magnetic property. The magnetic nanocomposites could be easily isolated from a matrix by using an external magnetic field instead of centrifuging or filtrating.[27–29] By encapsulating magnetic components into ion imprinted mesoporous silica, high molecular accessibility and specific recognition can be combined with magnetic properties to obtain a novel solid phase extraction material with highly selective recognition, large adsorption capacity, fast adsorption kinetics, and simple and rapid solid–liquid separation.[30–36]

In this work, we reported a novel magnetic ion imprinted mesoporous silica (MIIMS) nanocomposites with a magnetite (Fe_3O_4) core and highly ordered Cd^{2+} imprinted mesoporous silica shell *via* a simply co-condensation synthetic method. The synthesis procedure has been shown in Scheme 1. *N*-[3-(Trimethoxysilyl)propyl]ethylenediamine (AAPTS) and tetraethoxysilane (TEOS) were chosen as the functional monomer and cross-linker, respectively, while cetyltrimethylammonium bromide (CTAB) was used as the SDAs. The prepared MIIMS was characterized by small angle X-ray diffraction (XRD), transmission electron microscopy (TEM), nitrogen adsorption–desorption isotherms and vibrating sample magnetometer (VSM). Finally, its adsorption behavior in aqueous solutions was investigated and compared to magnetic non-imprinted mesoporous silica (MNIMS).

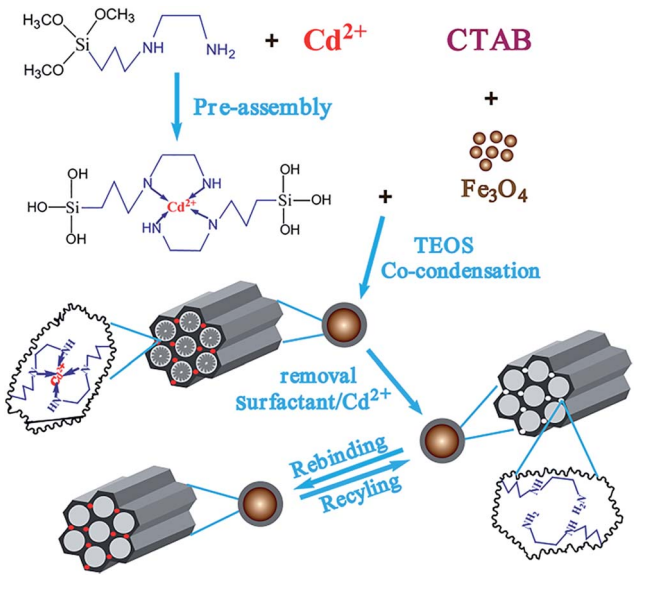

Scheme 1 Schematic procedure for synthesis of magnetic Cd^{2+} imprinted mesoporous silica (CTAB – cetyltrimethylammonium bromide, TEOS – tetraethoxysilane).

2. Materials and methods

2.1. Materials

Nano-iron oxide (Fe_3O_4, 99%) was purchased from Sima-lab company (Tianjin, China). Tetraethoxysilane (TEOS) and *N*-[3-(trimethoxysilyl)propyl]ethylenediamine (AAPTS) were obtained from Aladdin Reagent Company (Shanghai, China), while cetyltrimethylammonium bromide (CTAB) was purchased from Sinopharm Chemical Reagent Company (Shanghai, China). $CdCl_2 \cdot 2.5H_2O$, $Cu(NO_3)_2 \cdot 3H_2O$, $FeCl_3 \cdot 6H_2O$, $Pb(NO_3)_2$ and $MgCl_2 \cdot 6H_2O$ were acquired from Tianjin Chemical Reagent Company (Tianjin, China). Acetic acid, ethanol and concentrated ammonia aqueous solution (25 wt%) were purchased from Kermel (Tianjin, China). All chemicals were of analytical grade or better. Double deionized water (DDW) was used as the solvent and for conducting all rinses.

2.2. Preparation of MIIMS

In a one-step process, 55 mg $CdCl_2 \cdot 2.5H_2O$ and 220 mg AAPTS were dissolved in 10 mL DDW and stirred for 2 h at 60 °C to form a pre-assembly solution. Next, 0.53 g of CTAB and 2.8 g of ammonia aqueous solution (25 wt%) were dissolved in 110 mL of DDW and stirred at 30 °C. Then, 100 mg of Fe_3O_4 was added to this ammonia solution under vigorous stirring to form a homogeneous dispersion system. After stirring for 0.5 h, the pre-assembly solution was added to this mixture and stirred for another 0.5 h. Following that, 1.08 g TEOS was introduced dropwise into the mixture under vigorous stirring. The stirring was continued for 24 h. The MIIMS product was separated from the mixture by a magnet, and rinsed with ethanol and DDW. Any Cd^{2+} in the product was extracted by ethanol/HCl (9 : 1, v/v) solution to obtain the final MIIMS product. Magnetic non-imprinted mesoporous silica (MNIMS) was prepared using the same procedure but excluding $CdCl_2$.

2.3. Apparatus and analytical conditions

Small angle X-ray diffraction (XRD) measurements were conducted with Bruker D8 Advance Scattering system using Cu Kα (λ = 1.5405 Å) radiation over a range of 0.5–10° 2θ. Fourier transform infrared spectra (FTIR) were recorded using a Varian DRX-400 Fourier Transform Spectrophotometer. The target compounds were also characterized by transmission electron

microscope (TEM, Hitachi HT7700, Japan). N_2 adsorption–desorption measurements were carried out at 77 K using Belsorp-Max surface area and pore size analyzer. Surface areas were calculated by the Brunauer–Emmett–Teller (BET) method, and the pore volume and pore-size distributions were calculated using the Barret–Joyner–Halenda (BJH) model. Metal ion concentrations were recorded on a Varian 730 ES Inductive Coupled Plasma Emission Spectrometer.

2.4. Adsorption experiment

Adsorption experiments were carried out using 10 mg MIIMS or MNIMS and 10 mL solution at 25 °C. The pH of the solution was adjusted by using an acetic acid/sodium acetate buffer solution. For the pH test, MIIMS or MNIMS were added at different pH (2.0–6.0) of Cd^{2+} solution (300 mg L^{-1}) in each vial. The calculated imprinting factor (IF) was defined as $IF = B_i/B_n$, where B_i and B_n represented the binding capacity of MIIMS and MNIMS, respectively. After each adsorption cycle, the MIIMS or MNIMS were separated by a magnet, and the residual concentration of Cd^{2+} in the supernatant was measured. All the adsorption experiments were conducted in triplicate, and the mean values are reported.

A series of Cd^{2+} solutions in the range of 5 to 500 mg L^{-1} at pH 5.0 was used to investigate the isothermal adsorption experiments. The adsorption kinetics tests were performed using Cd^{2+} solutions of two different concentrations (30 and 300 mg L^{-1}). After shaking for regular time, the MIIMS was separated, and the residual concentration of Cd^{2+} in the solution was measured by ICP-MS.

In order to measure selectivity of the MIIMS, solutions of Cd^{2+}, Cu^{2+}, Pb^{2+}, Mg^{2+} and Fe^{3+} (1 mmol L^{-1}) were used, and the pH of each solution was maintained at 5.

2.5. Reusability and reproducibility

Cd^{2+} solution of concentration 300 mg L^{-1} at pH 5.0 was used for testing the reusability and reproducibility of the MIIMS. In each cycle, the Cd^{2+} absorbed by the MIIMS was eluted with 4 mL of 2 mol L^{-1} HCl. The MIIMS was washed thrice with DDW, neutralized with 1 M NaOH, again rinsed thrice with DDW, and dried. The dried MIIMS was then used for the next adsorption cycle. The same MIIMS was reused 6 times for adsorption of Cd^{2+} to measure its reusability. Additionally, five batches of MIIMS prepared at different times were employed to evaluate the reproducibility of MIIMS.

2.6. Removal of Cd^{2+} from water samples

Sample of mineral wastewater was collected in a polyethylene bottle from Shangba Dam (Guangdong, China) with pH 2.8 and Cd^{2+} concentration of 0.27 mg L^{-1}. The water sample was filtered through a 0.45 μm micro filtration membrane to remove all impurities, and the pH was adjusted to 5. Then, 100 mg of MIIMS was used to adsorb Cd^{2+} from 10 mL of the mineral wastewater. After shaking for 10 min, the MIIMS was separated and the residual concentration of Cd^{2+} in the solution was analyzed by ICP-MS. The recycle approach of the MIIMS was same as that of the reusability experiment mentioned above.

3. Results and discussion

3.1. Characterization of MIIMS

3.1.1. FT-IR spectra. Fig. 1a presents the FT-IR spectra of MIIMS before and after Soxhlet extraction. The absorbance peaks observed at 2920 cm^{-1} and 2850 cm^{-1} were attributed to the asymmetrical stretching and symmetrical stretching

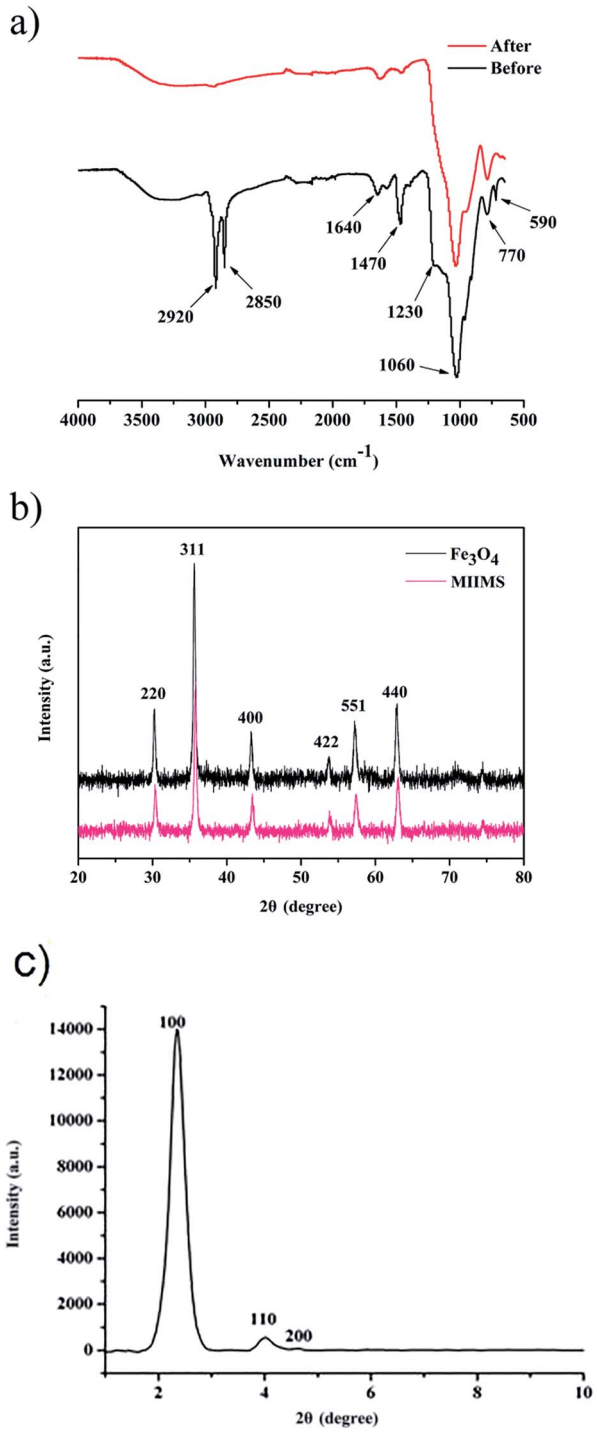

Fig. 1 (a) FT-IR spectra of MIIMS before and after Soxhlet extraction; (b) the wide-angle XRD patterns; (c) the low-angle XRD pattern of MIIMS.

vibration of CH_2, while the peak at 1470 cm^{-1} was attributed to the CH_2 in plane bending vibration.[37] The peaks for CH_2 decreased significantly after Soxhlet extraction, which confirmed that CTAB was extracted from the silica matrix. The appearance of NH_2 bending vibration at 1640 cm^{-1} verified that the γ-(aminoethylamino) propyl chelating group was successfully incorporated into the mesoporous silica. The peaks at 1230, 1060, 770 and 590 cm^{-1} were typical Si–O–Si bonds and showed that the MIIMS was mainly composed of silica material.

3.1.2. XRD patterns. The crystalline structure of MIIMS was analyzed by wide-angle XRD. As shown in Fig. 1b, the XRD patterns displayed several relatively strong reflection peaks in the 2θ region of 20–80°, with six characteristic peaks for Fe_3O_4 ($2\theta = 30.3°$, 35.7°, 43.5°, 53.4°, 57.3° and 62.9°) observed for the two samples. These peak positions indexed to (220), (311), (400), (422), (511) and (440) (JCPDS cards: 19-629). The XRD patterns revealed that the crystalline structures of the Fe_3O_4 in MIIMS were essentially maintained.

Low-angle XRD pattern of MIIMS is shown in Fig. 1c, three characteristic diffraction peaks of (100), (110) and (200) were observed, which revealed that the MIIMS owned a long range ordering of the porous structure and well-formed hexagonal pore arrays despite the embedding of iron oxide nanoparticles.

3.1.3. Morphological characteristics. TEM images (Fig. 2a) revealed that the MIIMS had a spherical morphology and a core–shell structure. The outer shells were much thinner than the interior magnetic cores, and the thicknesses of the mesoporous silica shells were observed to in the range of 3–5 nm.

3.1.4. BET analysis. The surface properties of the adsorbing material are significant for the adsorption of heavy metal cation. Fig. 2b shows the N_2 adsorption–desorption isotherms of the MIIMS, which corresponded to a type IV isotherm with a hysteresis loop, conforming its mesoporous characteristics. The inset picture in Fig. 2b presented the mean pore size, which was estimated by the Barret–Joyner–Halenda (BJH) method to be 3.23 nm. The Brunauer–Emmett–Teller (BET) surface area was 946 $m^2\ g^{-1}$ while the pore volume was 0.91 $cm^3\ g^{-1}$. All of these results confirmed the successful synthesis of MIIMS with a typical MCM-41 mesoporous shell.

3.1.5. Magnetic property analysis. Fig. 2c illustrates the magnetic hysteresis loop of naked Fe_3O_4 and MIIMS at 300 K. This result indicated that the sample was superparamagnetic,[38] which facilitated the magnetic separation and reusability. The saturation magnetization values of Fe_3O_4 and MIIMS were 76.48 emu g^{-1} and 28.48 emu g^{-1}, respectively. The inset picture manifested that although the magnetization value decreased after the assembling process, the MIIMS could respond to the external magnetic field and could be completely separated from aqueous solution conveniently.

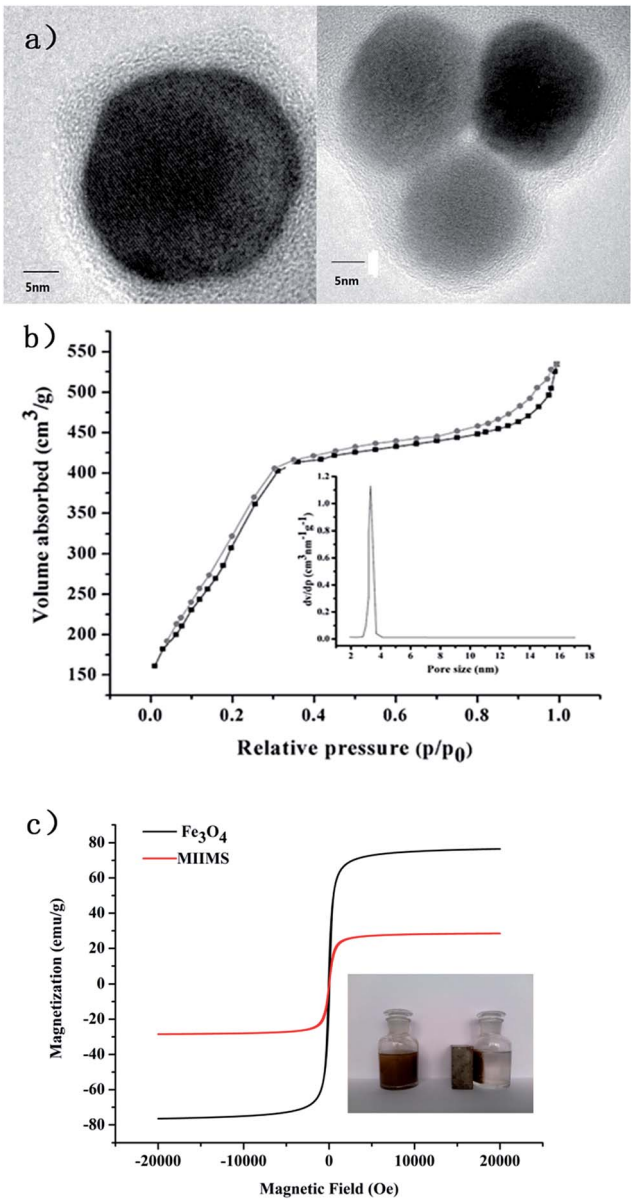

Fig. 2 (a) TEM image of MIIMS; (b) N_2 adsorption–desorption isotherm; (c) magnetization curves (inset picture: MIIMS suspended in DDW (left) and separated by an external magnet (right)).

3.2. Binding properties of MIIMS

The complexation between heavy metal ions and ligand diamine groups are strongly influenced by the ambient pH. Thus experiments were performed to explore the effects of solution pH on the adsorption capacity and imprinting factor (IF) of the MIIMS. Fig. 3 showed that the binding capacity of MIIMS toward Cd^{2+} was positively correlated with the pH (range from 2.0–6.0), while the IF showed a negative one. The largest adsorption capacity (approximately 29.1 mg g^{-1}) and IF (2.5) was observed at solution pH of 6.0 and 2.0, respectively. This could be attributed to the degree of protonation of the electron-donating nitrogen atoms in the Cd^{2+} imprinted cavities, which reduced the binding ability of the amino group involved in chelation with Cd^{2+}. However, MNIMS adsorbed Cd^{2+} through nonspecific binding, which was weak compared to the specific adsorption exhibited by the MIIMS (Fig. 4).

When the pH value was low, the binding capacity of MIIMS was small, while precipitation of the metal hydroxide was expected at a high pH. Accordingly, we measured the adsorption tests within a pH range of 2.0 to 6.0, for the purpose of

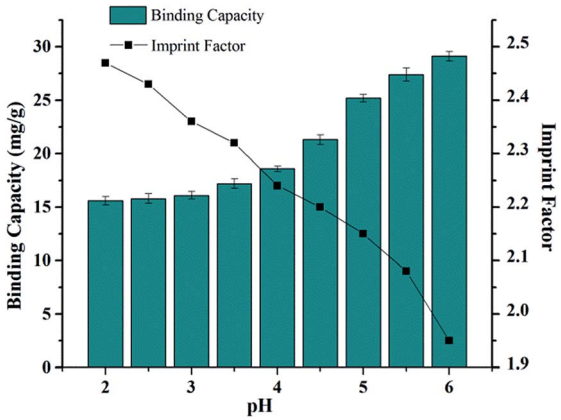

Fig. 3 The effect of pH on adsorption capacity and IF of MIIMS (experimental conditions: used 10 mL of 300 mg L^{-1} Cd^{2+} solution, solid weight 10 mg, $T = 298$ K).

estimating the optimum pH. Synthesizes the binding capacity and selectivity, we used an acetic acid/sodium acetate buffer solution with a pH of 5 for conducting subsequent adsorption tests.

Scatchard analysis (Fig. 5) was used to estimated the binding data for assess the adsorption properties of MIIMS. The Scatchard equation is as follows:

$$\frac{Q_e}{C_e} = \frac{Q_{max} - Q_e}{K_d} \quad (1)$$

where Q_e (mmol g^{-1}) is the equilibrium adsorption capacity, Q_{max} (mmol g^{-1}) is the apparent maximum adsorption capacity, C_e (mmol L^{-1}) is the equilibrium concentration of Cd^{2+}, and K_d (mmol L^{-1}) is the equilibrium dissociation constant. The Scatchard curve of MIIMS (Fig. 5a) could be modelled as two separate straight lines with different slopes, indicating that the MIIMS possessed two types of binding sites. Basing on the slope and intercept of fitting line, K_{d1} for the specific binding sites and K_{d2} for the nonspecific binding sites for MIIMS were 0.1116 mmol L^{-1} and 8.312 mmol L^{-1}. The Scatchard curve of

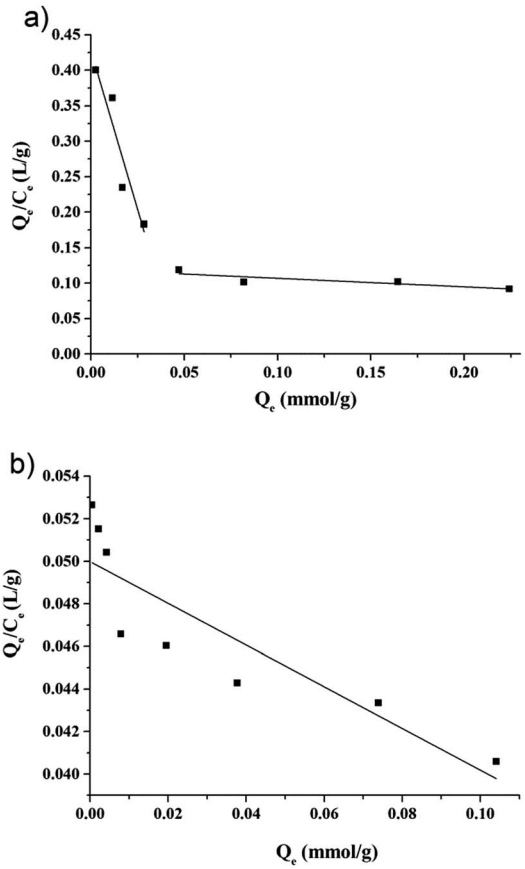

Fig. 5 Scatchard curve of MIIMS (a) and MNIMS (b).

MNIMS (Fig. 5b) could be modelled as one straight line, which indicated that there was only one type of binding site existing in the MNIMS, and the value of K_d is 10.20 mmol L^{-1}.

3.3. Kinetic study

Two different concentrations of Cd^{2+} solutions were used for the adsorption kinetic study of the MIIMS. The results (Fig. 6)

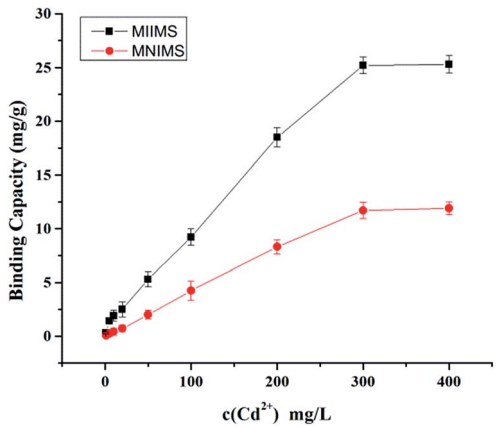

Fig. 4 Adsorption capacity of MIIMS and MNIMS (experimental conditions: used 10 mL of different concentrations of Cd^{2+} solution at pH 5.0, solid weight 10 mg, $T = 298$ K).

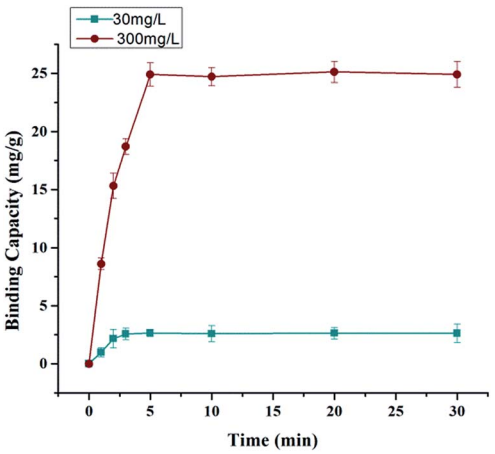

Fig. 6 Adsorption kinetics of MIIMS (used 10 mL solution at pH 5.0, 10 mg adsorbent, $T = 298$ K).

showed the equilibrium adsorption time is longer at high concentration of Cd^{2+}. For concentrations of 30 and 300 mg L^{-1}, the adsorption of Cd^{2+} reached equilibrium within 3.0 and 5.0 min, respectively. The times to reach adsorption equilibrium were much faster than that of a typical molecularly imprinted polymer adsorbent,[39,40] and it was basically in line with common imprinted mesoporous silica.[26] We believe that the nanometer-sized wall thicknesses and large pore size of the mesoporous silica allowed Cd^{2+} to readily access the imprinted sites.

To study the adsorption kinetics of Cd^{2+} onto MIIMS, pseudo-first-order and pseudo-second-order kinetic models were used. The pseudo-first-order kinetic model is as follows.

$$\log(Q_e - Q_t) = \log Q_e - k_1 t \quad (2)$$

The pseudo-second-order kinetic model is as follows.

$$\frac{t}{Q_t} = \frac{1}{k_2 Q_e^2} + \frac{t}{Q_e} \quad (3)$$

where t (min) is the adsorption time; Q_t (mg g^{-1}) and Q_e (mg g^{-1}) are the adsorption capacity at time t (min) and at the equilibrium, respectively. k_1 (min^{-1}) and k_2 (mg g^{-1} min^{-1}) are pseudo-first-order and pseudo-second-order rate constants of adsorption, respectively. The pseudo-second-order model (Fig. 7) was the best-fitting model because it gave higher correlation coefficient (>0.99) than the pseudo-first-order model (<0.90). Based on the pseudo-second-order model, it was assumed that the rate-limiting step may be chemical phenomena involving the electronic sharing of the Cd and the N of the functional monomer.

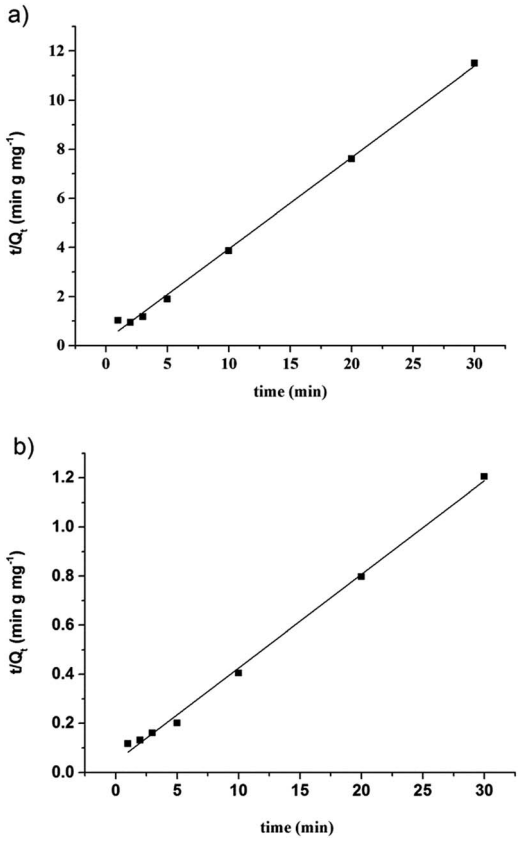

Fig. 7 The pseudo-second-order model of adsorption kinetics of MIIMS in solution (30 mg L^{-1} (a); 300 mg L^{-1} (b)).

3.4. Selectivity study

In order to further confirm that the obtained MIIMS nanoparticles can selectively recognize Cd^{2+}, even in a mixed solution containing other metal ions, we performed competitive adsorption study with Cu^{2+}, Pb^{2+}, Mg^{2+} and Fe^{3+}. These ions were chosen as they could coexist in wastewaters with Cd^{2+}, and they have same charge and similar ionic radius with Cd^{2+}. In addition, Fe^{3+} is a common ion in aquatic environments and is often detected at high concentrations in some water samples. As showed in Fig. 8, the adsorption capacities of MNIMS toward all the ions were not significantly different, while that of MIIMS to Cd^{2+} was much higher than its adsorption capacities toward Cu^{2+}, Pb^{2+}, Mg^{2+} or Fe^{3+}. The results indicated that the MIIMS possessed good selective recognition ability, which stem from the imprinting effect of the MIIMS. Note that MNIMS had almost no selectivity, which was due to the random distribution of the chelating ligands in the mesoporous silica.

3.5. Reusability and reproducibility

Reusability is a valuable attribute for economically viable adsorbent, and so we studied the reusability performance of MIIMS. Hydrochloric acid (4 mL, 2 mol L^{-1}) was utilized to elute the Cd^{2+} adsorbed by MIIMS for reuse. Fig. 9 indicated that MIIMS displayed good reusability without experiencing a marked decline in its adsorption capacity. The adsorption capacity of MIIMS reached 94.2% even after six cycles. However, the decrease of adsorption capacity of MIIMS is inevitable after many adsorption–regeneration cycles, which is a general feature of most imprinting polymers.[41]

The reproducibility also was investigated, and five batches of MIIMS prepared at different times were used. The relative standard deviations for the reproducibility of MIIMS were less

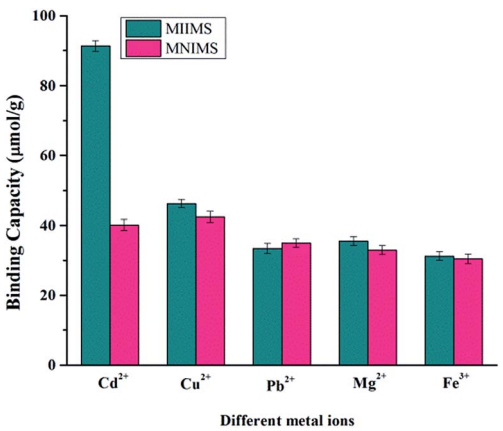

Fig. 8 Selective adsorption experiments of MIIMS and MNIMS (experimental conditions: initial concentrations of metal ions 1 mmol L^{-1}, 10 mL solution at pH 5.0, 10 mg adsorbent, $T = 298$ K).

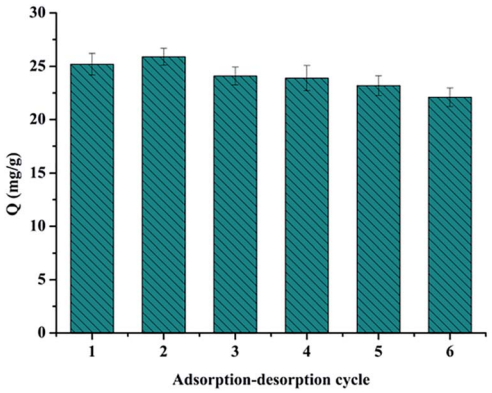

Fig. 9 Reusability of MIIMS (experimental conditions: 10 mL of 300 mg L^{-1} Cd^{2+} solution at pH 5.0, 10 mg adsorbent, $T = 298$ K).

than 4.2% between all the samples. The above results demonstrated that freshly synthesized magnetic mesoporous nanoparticles possessed satisfactory reusability and reproducibility performances.

3.6. Application of actual wastewater sample

To demonstrate the applicability of MIIMS to remove Cd^{2+} in real world sample, we collected the mineral wastewater from the Shangba Dam. The initial Cd^{2+} concentration in the mining effluent was 0.27 mg L^{-1} with a pH of 2.8. After the wastewater was adjusted to pH 5, and treated using 100 mg of MIIMS, the residual Cd^{2+} concentrations decreased to 0.03 mg L^{-1}. By adding 10 g of MIIMS to per liter of the mining effluent, the concentration of Cd^{2+} was less than the discharge standard (0.1 mg L^{-1}) of China.

4. Conclusions

In this paper, we introduced a set of procedures to fabricate magnetic ion imprinted mesoporous silica core shell nanocomposites with highly ordered periodic structure *via* a co-condensation method. The MIIMS combined the advantages of molecularly imprinted polymers, mesoporous silica materials, and magnetic materials. The MIIMS remains highly selective recognition, high adsorption capacity (25.2 mg g^{-1}) and rapid adsorption kinetics (reach equilibrium within 4.5 min). By encapsulating magnetic core into ion imprinted mesoporous silica, MIIMS is quite easy to be separated and recycled, which makes it a novel solid phase extraction adsorbent. Therefore, it is convenient to apply MIIMS for the wasterwater treatment to remove cadmium presented in mineral effluent effectively and efficiently. Besides, this synthetic approach was simple, effective, economic, safe, environment friendly, and processes a good reproducibility, so it could also be used to prepare other metal ions imprinted mesoporous silica magnetic adsorbents. The wastewater treatment applications show that the concentration of Cd^{2+} was lower than the discharge standard of China, resulting from the usage of MIIMS. However, the decrease of adsorption capacity of MIIMS is inevitable after many adsorption–regeneration cycles, which needs further researches.

Acknowledgements

We gratefully acknowledge the financial support from the NSFC-GD Joint Foundation of the Key Projects (No. U1201234) and National Natural Science Foundation of China (No. 21275057).

References

1 K. F. Lam, K. L. Yeung and A. G. Mckay, *Environ. Sci. Technol.*, 2007, **41**, 3329–3334.
2 P. N. Williams, M. Lei, G. X. Sun, Q. Huang, Y. Lu, C. Deacon, A. A. Meharg and Y. G. Zhu, *Environ. Sci. Technol.*, 2009, **43**, 637–642.
3 E. Álvarez-Ayuso and A. García-Sánchez, *J. Hazard. Mater.*, 2007, **147**, 594–600.
4 N. Meunier, P. Drogui, C. Montané, R. Hausler, G. Mercier and J. F. Blais, *J. Hazard. Mater.*, 2006, **137**, 581–590.
5 M. Y. Vilensky, B. Berkowitz and A. Warshawsky, *Environ. Sci. Technol.*, 2002, **36**, 1851–1855.
6 K. L. Huang, T. M. Holsen, T. C. Chou and J. R. Selman, *Environ. Sci. Technol.*, 2003, **37**, 1992–1998.
7 C. A. Bashaa, M. Somasundaramb, T. Kannadasanb and C. W. Lee, *Chem. Eng. J.*, 2011, **171**, 563–571.
8 J. Gao, S. P. Sun, W. P. Zhu and T. S. Chung, *Water Res.*, 2014, **63**, 252–261.
9 Y. Zhang, Y. Chen, C. Wang and Y. Wei, *J. Hazard. Mater.*, 2014, **276**, 129–137.
10 C. Han, W. Cai, W. Tang, G. Wang and C. Liang, *J. Mater. Chem. A*, 2011, **21**, 11188–11196.
11 Y. K. Seo, J. W. Yoon, J. S. Lee, Y. K. Hwang, C. H. Jun, J. S. Chang, S. Wuttke, P. Bazin, A. Vimont, M. Daturi, S. Bourrelly, P. L. Llewellyn, P. Horcajada, C. Serre and G. Férey, *Adv. Mater.*, 2012, **24**, 806–810.
12 M. A. Barakat, *Arabian J. Chem.*, 2011, **4**, 361–377.
13 L. X. Zhang, H. Y. Niu, W. H. Li, Y. L. Shi and Y. Q. Cai, *Chem. Commun.*, 2011, **47**, 4454–4456.
14 L. Zhang, S. Qiao, Y. Jin, H. Yang, S. Budihartono, F. Stahr, Z. Yan, X. Wang, Z. Hao and G. Lu, *Adv. Funct. Mater.*, 2008, **18**, 3203–3212.
15 Q. Meng, X. Zhang, C. He, G. He, P. Zhou and C. Duan, *Adv. Funct. Mater.*, 2010, **20**, 1903–1909.
16 C. Kang, W. Li, L. Tan, H. Li, C. Wei and Y. Tang, *J. Mater. Chem. A.*, 2013, **1**, 7147–7153.
17 H. Liu and W. Chen, *RSC Adv.*, 2015, **5**, 27034–27042.
18 L. Chem, X. Wang, W. Lu, X. Wu and J. Li, *Chem. Soc. Rev.*, 2016, **45**, 2137–2211.
19 Y. Cai, L. Zheng and Z. Fang, *RSC Adv.*, 2015, **5**, 97435–97445.
20 M. Razali, J. F. Kim, M. Attfield, P. M. Budd, E. Drioli, Y. M. Lee and G. Szekely, *Green Chem.*, 2015, **17**, 5196–5205.
21 S. Dai, M. C. Burleigh, Y. Shin, C. C. Morrow, C. E. Barnes and Z. L. Xue, *Angew. Chem., Int. Ed.*, 1999, **38**, 1235–1239.
22 J. Tan, H. F. Wang and X. P. Yan, *Anal. Chem.*, 2009, **81**, 5273–5280.

23 S. Xu and H. Lu, *Chem. Commun.*, 2015, **51**, 3200–3202.
24 K. Suzuki, K. Ikari and H. Imai, *J. Am. Chem. Soc.*, 2004, **126**, 462–463.
25 W. Zhao, J. Gu, L. Zhang, H. Chen and J. Shi, *J. Am. Chem. Soc.*, 2005, **127**, 8916–8917.
26 R. He, W. Li, D. Deng, W. Chen, H. Li, C. Wei and Y. Tang, *J. Mater. Chem. A*, 2015, **3**, 9789–9798.
27 J. Kim, H. S. Kim, N. Lee, T. Kim, H. Kim, T. Yu, I. C. Song, W. K. Moon and T. Hyeon, *Angew. Chem., Int. Ed.*, 2008, **47**, 8438–8441.
28 Q. Yuan, N. Li, Y. Chi, W. Geng, W. Yan, Y. Zhao, X. Li and B. Dong, *J. Hazard. Mater.*, 2013, **254**, 157–165.
29 S. W. Jun, M. Shokouhimehr, D. J. Lee, Y. J. Jang, J. Park and T. Hyeon, *Chem. Commun.*, 2013, **49**, 7821–7823.
30 Y. Deng, D. Qi, C. Deng, X. Zhang and D. Zhao, *J. Am. Chem. Soc.*, 2008, **130**, 28–29.
31 G. Cheng, J. Zhang, Y. Liu, D. Sun and J. Ni, *Chem. Commun.*, 2011, **47**, 5732–5734.
32 L. Zhang, T. Wang, L. Li, C. Wang, Z. Su and J. Li, *Chem. Commun.*, 2012, **48**, 8706–8708.
33 S. Gai, P. Yang, P. Ma, D. Wang, C. Li, X. Li, N. Niu and J. Lin, *J. Mater. Chem. A*, 2011, **21**, 16420–16426.
34 C. Wang, S. Tao, W. Wei, C. Meng, F. Liu and M. Han, *J. Mater. Chem.*, 2010, **20**, 4635–4641.
35 X. Xin, Q. Wei, J. Yang, L. Yan, R. Feng, G. Chen, B. Du and H. Li, *Chem. Eng. J.*, 2012, **184**, 132–140.
36 O. Hakami, Y. Zhang and C. J. Banks, *Water Res.*, 2012, **46**, 3913–3922.
37 A. Benhamou, M. Baudu, Z. Derriche and J. P. Basly, *J. Hazard. Mater.*, 2009, **171**, 1001–1008.
38 S. Y. Xu, C. J. Guo, Y. X. Li, Z. R. Yu, C. H. Wei and Y. W. Tang, *J. Hazard. Mater.*, 2014, **264**, 34–41.
39 S. Piszkiewicz, E. A. Kirkbride, N. D. Stearns, B. R. Henderson, M. A. Lenker, E. Tang, L. H. Kawashiri, C. S. Nichols, S. C. Moore and S. G. Sogo, *Chem. Commun.*, 2013, **49**, 5954–5956.
40 T. Chang, Y. Liu, X. Yan, S. Liu and H. Zheng, *RSC Adv.*, 2016, **6**, 66297–66306.
41 J. Kupai, M. Razali, S. Buyuktiryaki, R. Kecili and G. Szekely, *Polym. Chem.*, 2017, DOI: 10.1039/c6py01853j.